Modeling Permeation of CO_2/CH_4, CO_2/N_2, and N_2/CH_4 Mixtures Across SAPO-34 Membrane with the Maxwell−Stefan Equations

Shiguang Li,[†] John L. Falconer,[†] Richard D. Noble,[†] and R. Krishna*[,‡]

Department of Chemical and Biological Engineering, University of Colorado, Boulder, Colorado 80309-0424, and Van't Hoff Institute for Molecular Sciences, University of Amsterdam, Nieuwe Achtergracht 166, 1018 WV Amsterdam, The Netherlands

The objective of this paper is test the capability of the Maxwell−Stefan (M−S) diffusion formulation to predict binary mixture permeation fluxes across a SAPO-34 membrane using only data on pure-component adsorption isotherms and diffusivities. Experiments were carried out for permeation of CO_2/CH_4, CO_2/N_2, and N_2/CH_4 mixtures across a SAPO-34 membrane with upstream pressures ranging to 7.2 MPa, ensuring that high occupancies within the zeolite layer are reached. Good agreement between the M−S mixture model and experiments are obtained provided the binary exchange coefficients $Đ_{12}$ in the M−S equations are assumed to have high enough values to ensure that intercage hops of the species occur independently of one other.

1. Introduction

The Maxwell−Stefan (M−S) equations[1−3]

$$-\rho\frac{q_i}{RT}\frac{\mathrm{d}\mu_i}{\mathrm{d}z}=\sum_{\substack{j=1\\ j\neq i}}^{n}\frac{q_jN_i-q_iN_j}{q_{j,\mathrm{sat}}Đ_{ij}}+\frac{N_i}{Đ_i};\quad i=1,\ldots,n \qquad (1)$$

are widely used in practice for modeling mixture diffusion in zeolites and carbon nanotubes. In eq 1, $Đ_i$ is the Maxwell−Stefan diffusivity of species i, q_i is the molar loading, $q_{i,\mathrm{sat}}$ is the saturation capacity of species i, and $Đ_{ij}$ are the binary exchange coefficients. Equation 1 has been widely used for modeling and interpretation of zeolite membrane permeation experiments for a variety of molecules and mixtures.[4−6] The major advantage of using the M−S equations is that the diffusion coefficients $Đ_i$ and $Đ_{ij}$ can be estimated from pure-component adsorption and diffusion data.[2,3] In recent years, there has been considerable interest in the use of zeolite membranes for separation of CO_2 and CH_4 mixtures,[7−9] and in two recent publications, Zhu et al.[9] and Li et al.[8] have modeled permeation of CO_2 (1)−CH_4 (2) mixtures across MFI and SAPO-34 (an isotype of CHA) membranes, respectively, making two debatable assumptions. First, in both papers the M−S diffusivity $Đ_i$ is assumed to be independent of the loading. Second, the binary exchange parameter $Đ_{12}$ is estimated using the interpolation formula.

$$Đ_{12}=[Đ_1]^{q_1/(q_1+q_2)}[Đ_2]^{q_2/(q_1+q_2)} \qquad (2)$$

Both these assumptions have been questioned in a recent paper by Krishna et al.[10] By reanalysis of *unary* permeation data of permeation of CO_2 and CH_4 across MFI, SAPO-34, and DDR membranes, Krishna et al.[10] demonstrated that the M−S diffusivity can be a strong function of the loading for a given guest molecule−host zeolite combination. Using molecular dynamics (MD) simulations as a basis, Krishna et al.[10,11] argued that, for zeolite structures that consist of cages separated by narrow windows, such as CHA, DDR, LTA, and ERI, intercage jumps are uncorrelated and, as an approximation, the binary exchange coefficient $Đ_{12}$ can be taken to be infinite, i.e.,

$$N_i=-\rho Đ_i\frac{q_i}{RT}\frac{\mathrm{d}\mu_i}{\mathrm{d}z};\quad i=1,\ldots,n \qquad (3)$$

However, the validity of eq 3 to describe mixture permeation in a cage-type zeolite membrane has not been tested against an experiment.

The present paper has the major objective of examining the extent to which eq 3 is successful for *quantitative* modeling of permeation of CO_2/CH_4, CO_2/N_2, and N_2/CH_4 mixtures across a SAPO-34 membrane using only *pure*-component isotherms and permeation data as inputs. For this purpose, dedicated experiments in an improved membrane were performed with upstream pressures ranging to 7.2 MPa in order to ensure high occupancies in the membrane and thus allowing the M−S equations to be tested more stringently. The membrane synthesis procedure used in the present study used a seeding procedure that resulted in a thinner membrane and higher fluxes than obtained in the previous study.[8] The details of membrane synthesis, characterization, and measurement procedures along

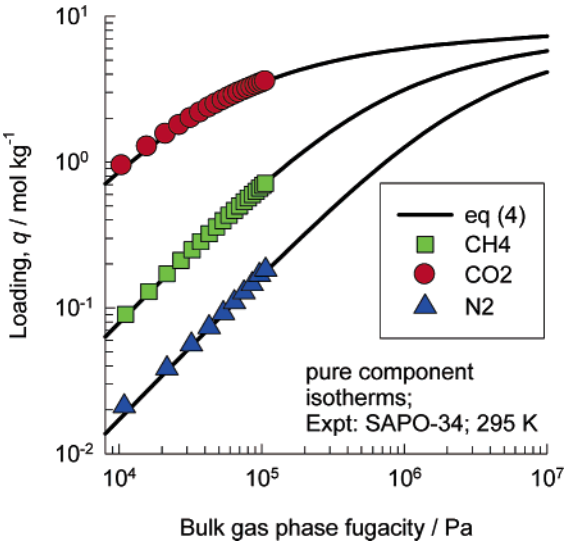

Figure 1. Pure-component isotherm data for CO_2, CH_4, and N_2 along with fits using eq 4, denoted by the continuous solid lines.

* Corresponding author. Fax: + 31 20 5255604. E-mail: r.krishna@uva.nl.

[†] University of Colorado.

[‡] University of Amsterdam.

10.1021/ie0610703 CCC: $37.00
Published on Web 10/28/2006

Table 1. Pure-Component Isotherm Fit Data Using Equation 4[a]

molecule	b_i	Ω_i	$q_{i,sat}$
CO_2	7.67×10^{-5}	6	8.2
CH_4	5.87×10^{-6}	6	8.2
N_2	1.26×10^{-6}	6	8.2

[a] b_i is expressed in Pa^{-1}, Ω_i is expressed in molecules/cage, and $q_{i,sat}$ is expressed in mol kg^{-1}.

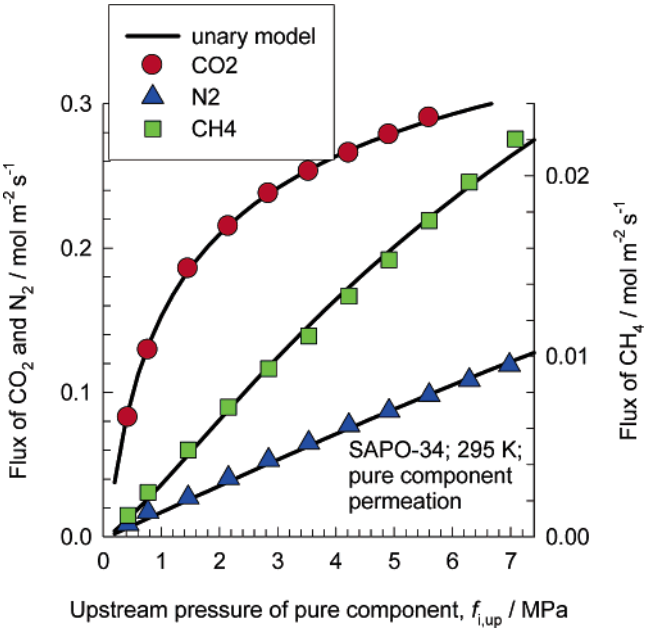

Figure 2. Unary permeation fluxes for CO_2, CH_4, and N_2 as a function of the upstream pressure. Also shown with continuous solid lines are the calculations using eqs 11 and 12 taking $\phi_i = 2.1$, 3.0, and 2.3 for CO_2, CH_4, and N_2 respectively. The values of the zero-loading transport coefficients $\rho Đ_i(0)/\delta = 4.6 \times 10^{-3}$, 3.2×10^{-4}, and 0.0107 kg m^{-2} s^{-1} for CO_2, CH_4, and N_2, respectively.

with the experimental data have been given in Appendix A of the Supporting Information accompanying this publication.

2. Fitting of Pure-Component Isotherms

The experimental pure-component isotherms for pure CO_2, CH_4, and N_2 at 295 K are plotted in Figure 1. For adsorption in zeolite structures with cages separated by narrow windows, such as SAPO-34, the model based on statistical thermodynamics described by Ruthven (Chapter 3)[12] is particularly relevant and useful.

$$q_i = \frac{q_{i,sat}}{\Omega_i} \frac{b_i f_i + \sum_{m=2}^{\Omega_i} \frac{(b_i f_i)^m}{(m-1)!} \left[\frac{1 - \frac{m}{\Omega_i + 1}}{1 - \frac{1}{\Omega_i + 1}}\right]^m}{1 + b_i f_i + \sum_{m=2}^{\Omega_i} \frac{(b_i f_i)^m}{(m)!} \left[\frac{1 - \frac{m}{\Omega_i + 1}}{1 - \frac{1}{\Omega_i + 1}}\right]^m} \quad (4)$$

In eq 4, q_i represents the loading in mol kg^{-1}, $q_{i,sat}$ is the saturation loading, and Ω_i is maximum capacity in molecules per cage. As explained in Appendix B of the Supporting Information, there are distinct advantages to using eq 4 for fitting isotherms in cage structures such as CHA and DDR.

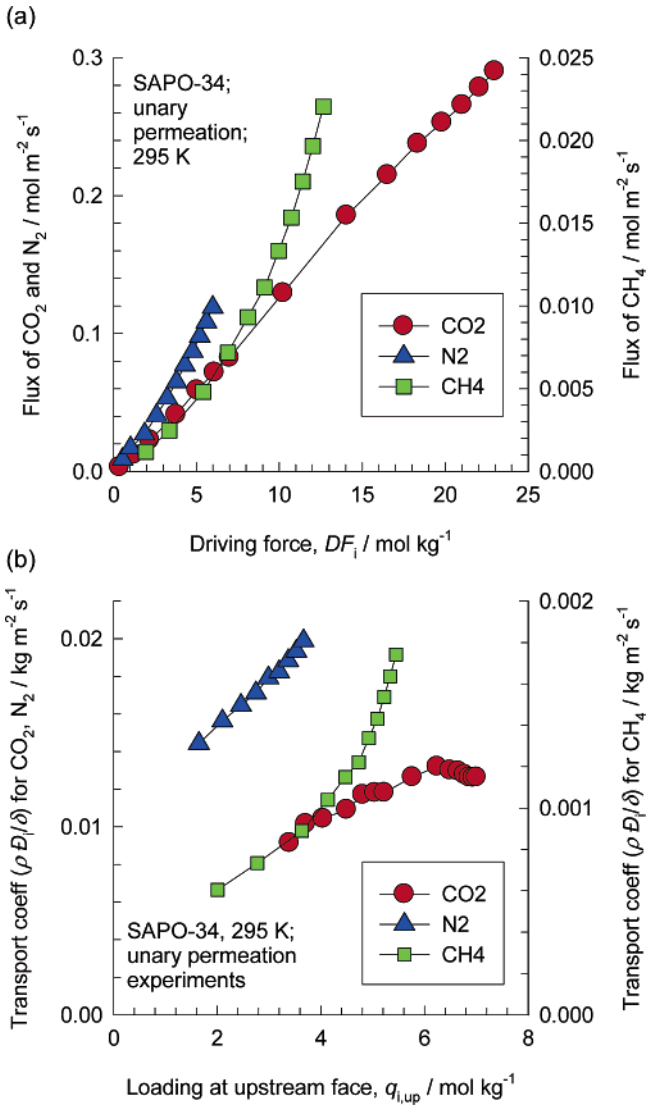

Figure 3. (a) Experimental data on unary permeation fluxes are plotted against the driving force DF_i, calculated from eq 8. (b) Transport coefficients, $\rho Đ_i/\delta$ backed out using eq 6, are shown as a function of the loadings at the upstream face of the membrane, $q_{i,up}$.

On the basis of the atomic composition of SAPO-34 used in our experiments, we calculate

$$q_{i,sat} = 1.369\Omega_i \quad (5)$$

It is important to have a good estimate of the saturation capacity, but it is not possible to obtain this information from experimental isotherm data because the pressures at which the pores get saturated can range to $\sim 10^9$ Pa and our experimental isotherms were only determined to a maximum pressure of 106 kPa. For CO_2, for example, the molar volume of the liquid phase at 10^9 Pa is estimated to lie in the range of 30−35 cm^3/mol from the data given by Mäder and Berman.[13] Golden and Sircar[14] estimate the molar volumes for CO_2, CH_4, and N_2 to be 33.3, 37.7, and 31.6 cm^3/mol, respectively. For the measured pore volume of 0.26 cm^3/g, the maximum capacity is estimated to be, after rounding off to integer values, 6 molecules/cage for CO_2, CH_4, and N_2; see Table 1 that also lists the values of the fit parameter b_i.

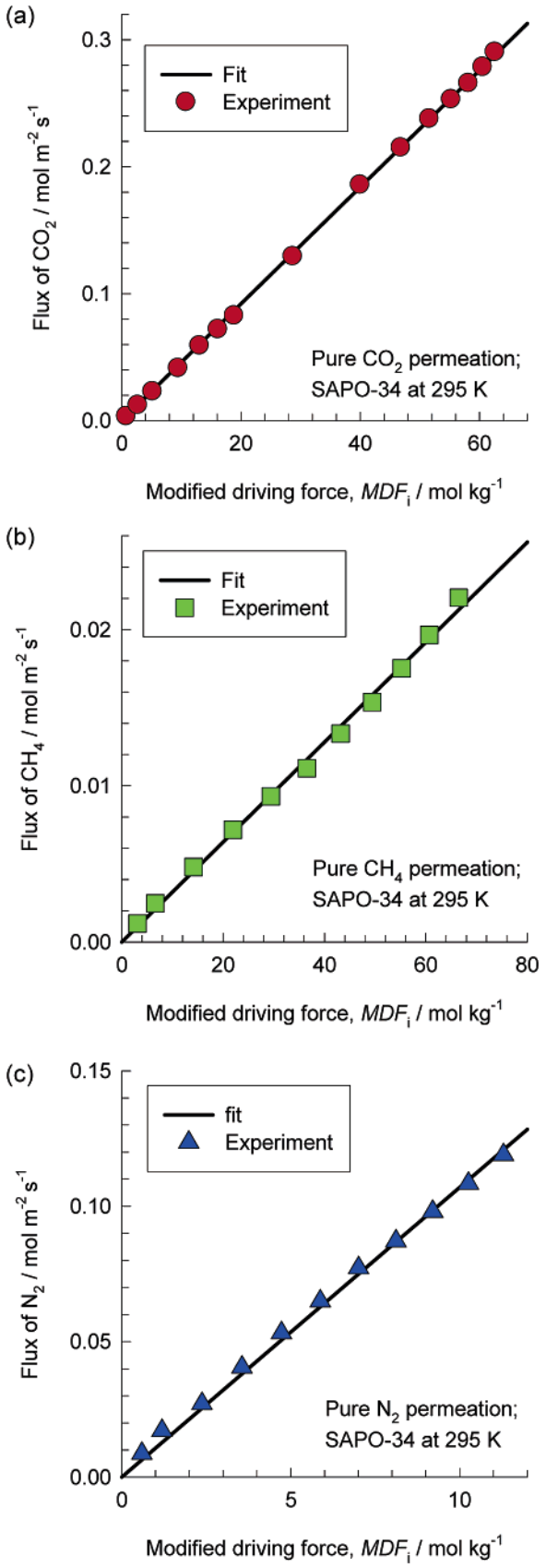

Figure 4. Experimental data on unary permeation fluxes of (a) CO_2, (b) CH_4, and (c) N_2 is plotted against the modified driving force MDF_i, calculated from eq 11, taking $\phi_i = 2.1$, 3.0, and 2.3 for CO_2, CH_4, and N_2, respectively. The straight line is drawn using eq 12 with fitted values of $\rho Đ_i(0)/\delta = 4.6 \times 10^{-3}$, 3.2×10^{-4}, and 0.0107 kg m^{-2} s^{-1} for CO_2, CH_4, and N_2, respectively.

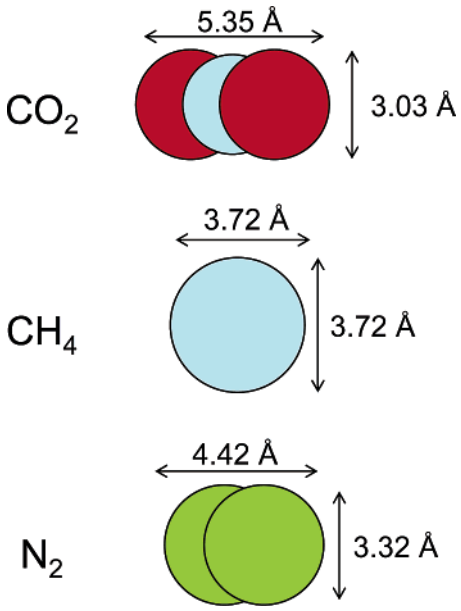

Figure 5. Illustration showing the approximate molecular dimensions of CO_2, CH_4, and N_2.

3. Analysis of Unary Permeation Data

The unary permeation fluxes for CO_2, CH_4, and N_2 at 295 K are plotted in Figure 2 as a function of the upstream pressure. If the M−S diffusivity can be taken to be loading independent, we may write the permeation flux as

$$N_i = \frac{\rho Đ_i}{\delta} \mathrm{DF}_i \tag{6}$$

where DF_i is the driving force

$$\mathrm{DF}_i \equiv \int_{f_{i,\mathrm{down}}}^{f_{i,\mathrm{up}}} \frac{q_i}{f_i} \mathrm{d}f_i \tag{7}$$

where $f_{i,\mathrm{up}}$ and $f_{i,\mathrm{down}}$ represent the pressures (more strictly, fugacities) of component i at the upstream (retentate) and downstream (permeate) sides of the membrane, respectively. The integral can be evaluated analytically to obtain

$$\mathrm{DF}_i = \frac{q_{i,\mathrm{sat}}}{\Omega_i} \ln\left(\frac{1 + b_i f_{i,\mathrm{up}} + \sum_{m=2}^{\Omega_i} \frac{(b_i f_{i,\mathrm{up}})^m}{(m)!} \left[\frac{1 - \frac{m}{\Omega_i + 1}}{1 - \frac{1}{\Omega_i + 1}} \right]^m}{1 + b_i f_{i,\mathrm{down}} + \sum_{m=2}^{\Omega_i} \frac{(b_i f_{i,\mathrm{down}})^m}{(m)!} \left[\frac{1 - \frac{m}{\Omega_i + 1}}{1 - \frac{1}{\Omega_i + 1}} \right]^m} \right) \tag{8}$$

Plots of the unary permeation fluxes for CO_2, CH_4, and N_2 against the driving force DF_i are shown in Figure 3a. For both CH_4 and N_2, there are significant departures from linearity. For CO_2, the dependence of the flux N_i on DF_i is observed to be nearly linear for low values of the driving force, but at higher DF_i, there appears to be significant departures from linearity.

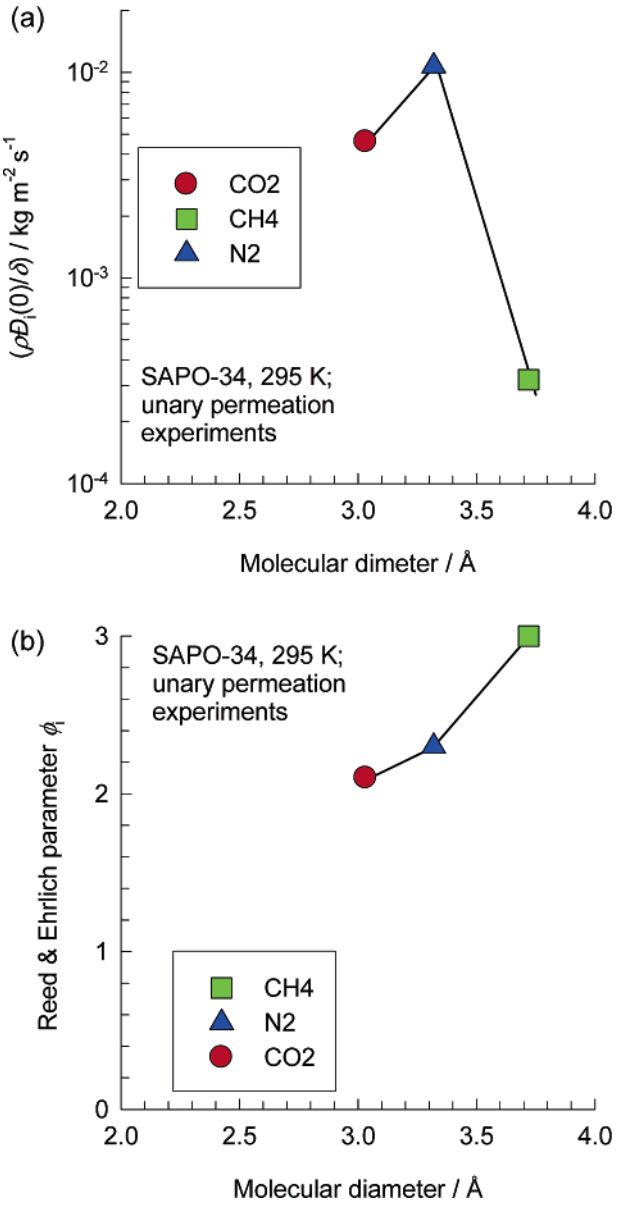

Figure 6. Dependence of the (a) the zero-loading transport coefficient $\rho Đ_i(0)/\delta$ and (b) the Reed and Ehrlich parameter ϕ_i on the molecular diameter.

For all three molecules, the assumption of a loading-independent $Đ_i$ appears to be unjustified; this is more clearly evident when the values of the transport coefficients, $\rho Đ_i/\delta$ backed out using eq 6, are plotted against the component loading at the upstream face of the membrane, $q_{i,up}$. The transport coefficients of CO_2, CH_4, and N_2 depend on the upstream loading; see Figure 3b.

To quantify the loading dependence, we use the model developed by Reed and Ehrlich;[10,15,16] this model gives the following expression,

$$Đ_i = Đ_i(0)\frac{(1+\epsilon_i)^{z-1}}{(1+\epsilon_i/\phi_i)^z} \tag{9}$$

where z is the coordination number, representing the maximum number of neighbors within a cage; we take $z = 5$, i.e., one less than the maximum capacity of molecules that can be accommodated in each cage. The other parameters are defined

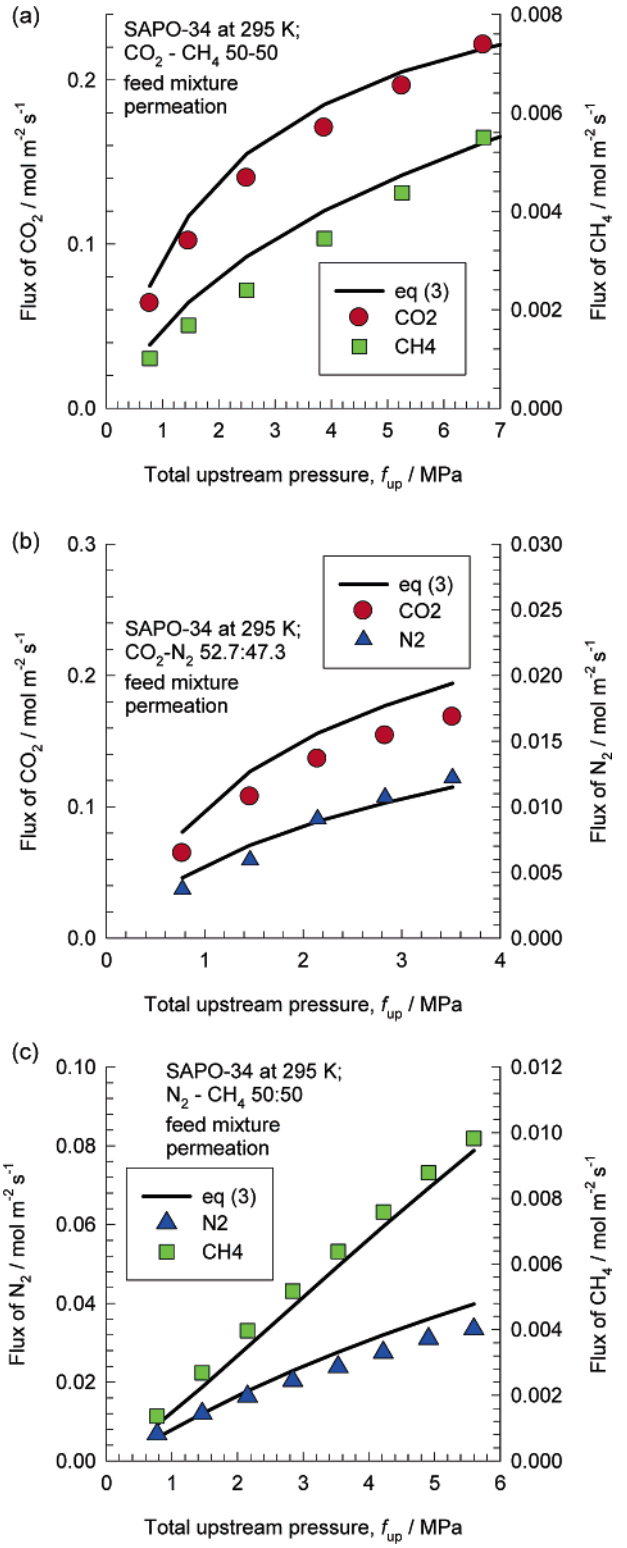

Figure 7. Permeation fluxes for binary (a) CO_2/CH_4, (b) CO_2/N_2, and (c) N_2/CH_4 mixtures as functions of the upstream total pressure, f_{up}. The continuous solid lines represent the calculations by numerical solution of eq 3 across the membrane.

as (see ref 10 for more detailed discussions and derivations)

$$\epsilon_i = \frac{(\beta_i - 1 + 2\theta_i)\phi_i}{2(1-\theta_i)}; \quad \beta_i = \sqrt{1 - 4\theta_i(1-\theta_i)(1-1/\phi_i)}; \quad \theta_i = \frac{q_i}{q_{i,sat}} \tag{10}$$

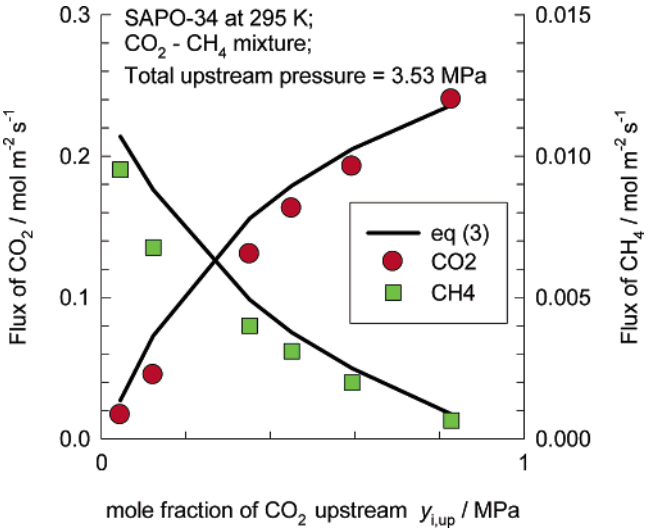

Figure 8. Permeation fluxes for CO_2 and CH_4 for mixture campaign in which the total upstream pressure was maintained constant at 3.53 MPa and the partial pressures of both components were varied. The continuous solid lines represent the calculations by numerical solution of eq 3 across the membrane.

With the Reed−Ehrlich loading dependence, we may define a modified driving force MDF_i

$$MDF_i \equiv \int_{f_{i,down}}^{f_{i,up}} \frac{(1+\epsilon_i)^{z-1}}{(1+\epsilon_i/\phi_i)^z} \frac{q_i}{f_i} df_i \qquad (11)$$

The integration must be carried out numerically. The modified driving force must be expected to bear a linear relation with the permeation flux

$$N_i = \frac{\rho Đ_i(0)}{\delta} MDF_i \qquad (12)$$

The plots for CO_2, CH_4, and N_2 are shown in Figure 4 parts a, b, and c, respectively. The Reed−Ehrlich parameter ϕ_i was chosen to yield a straight-line relationship; the best-fit values that yield *linear* dependencies of N_i on MDF_i are $\phi_i = 2.1$, 3.0, and 2.3 for CO_2, CH_4, and N_2, respectively.

Figure 5 presents illustrations showing approximate molecular dimensions of CO_2, CH_4, and N_2; these dimensions were estimated using published force fields for molecule−molecule interactions.[11,17,18] The values of the zero-loading transport coefficients $\rho Đ_i(0)/\delta$ appear to decrease sharply as the molecular diameter approaches the window size, which has a value of 3.8 Å for SAPO-34; see Figure 6a. The $\rho Đ_i(0)/\delta$ value for CO_2 is lower than that of N_2, perhaps because CO_2 is a longer molecule. The loading dependence, characterized by the parameter ϕ_i, is stronger when the molecular diameter is larger; see Figure 6b. For an interpretation of the loading dependence of the M−S diffusivity in terms of the free energy barrier for hopping of molecules between cages, see the papers of Beerdsen et al.[19,20]

4. Modeling of Binary Mixture Permeation

The experimental fluxes for binary (a) CO_2/CH_4, (b) CO_2/N_2, and (c) N_2/CH_4 mixtures are shown in Figures 7 parts a, b, and c (filled solid symbols), respectively, as a function of the total upstream pressure, f_{up}. The feed gas composition for the CO_2/CH_4 and N_2/CH_4 mixtures was precisely equimolar. For the CO_2/N_2 mixtures, the feed gas composition was in the proportion 52.7% and 47.3%. The set of two differential

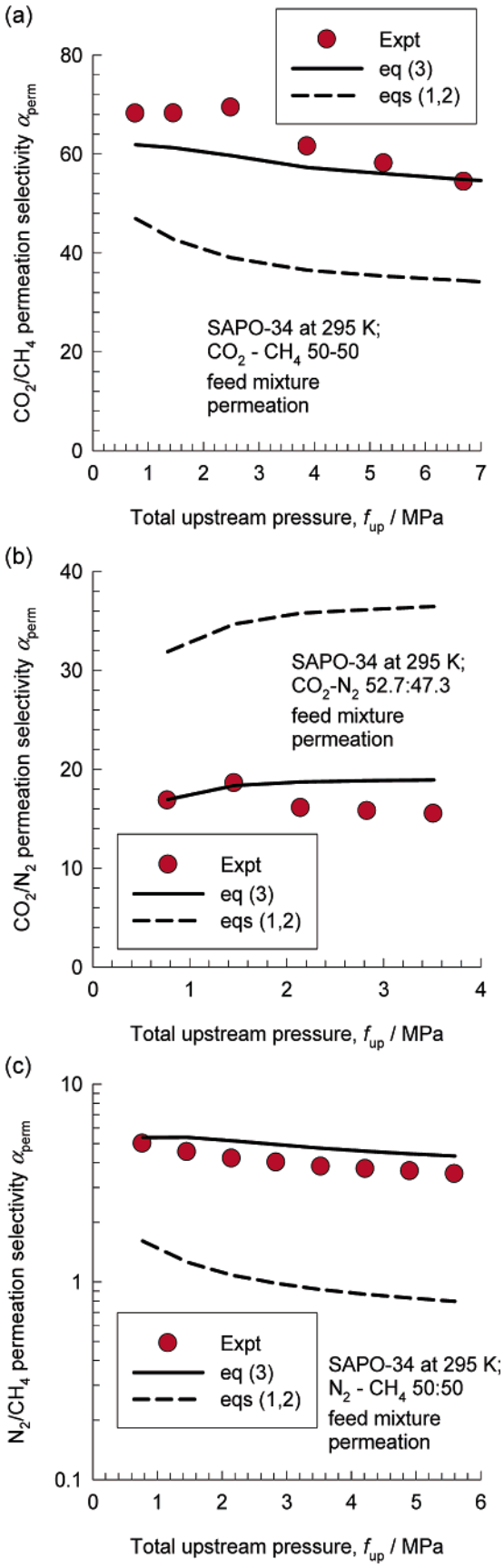

Figure 9. Permeation selectivity α_{perm} for binary (a) CO_2/CH_4, (b) CO_2/N_2, and (c) N_2/CH_4 mixtures as functions of the upstream total pressure, f_{up}. The continuous solid lines represent the calculations by numerical solution of eq 3 across the membrane. The dashed lines represent calculations using eqs 1 and 2.

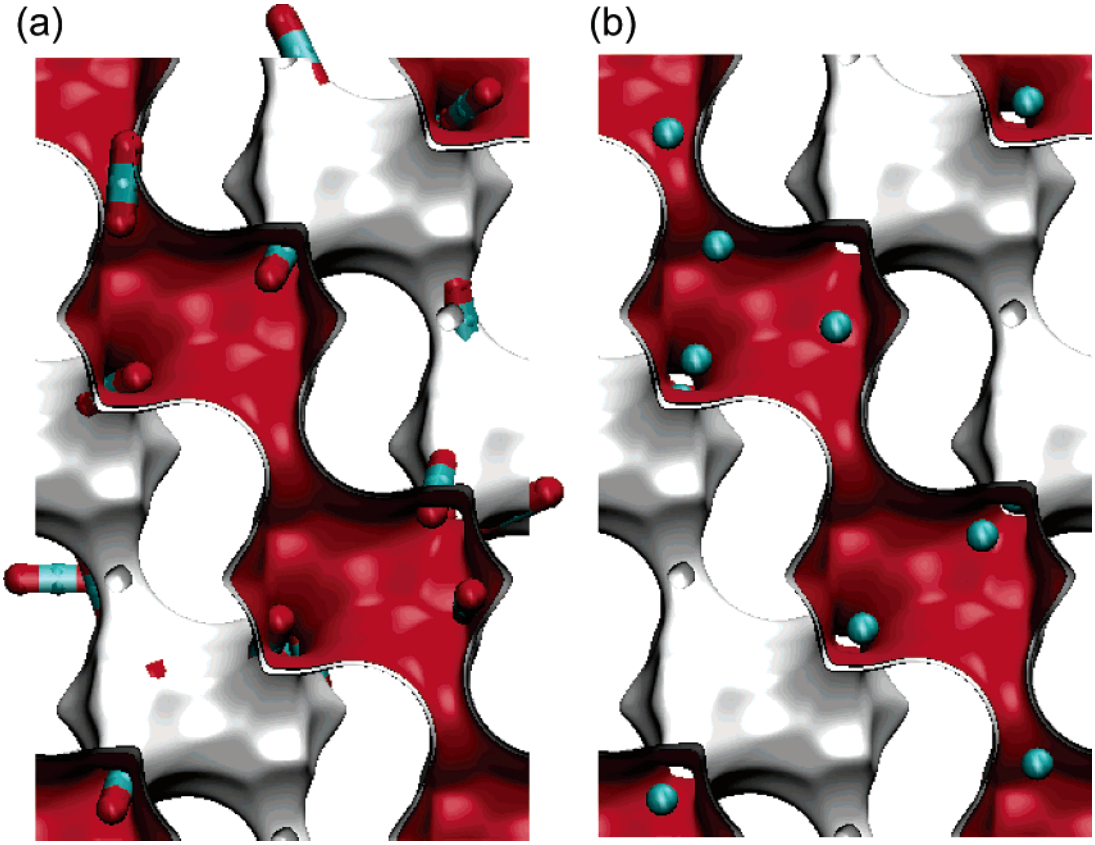

Figure 10. Snapshots showing the location of (a) CO_2 and (b) CH_4 molecules within the cages of SAPO-34 at 300 K and 1000 MPa.

equations (eq 3) across the membrane was integrated across the membrane to obtain the steady-state fluxes using the numerical procedure described in earlier work.[6,21] The mixture thermodynamics was estimated using the ideal adsorbed solution theory of Myers and Prausnitz.[22] The model calculations are indicated by continuous solid lines in Figure 7. For all three binary mixtures, the fluxes are predicted with good accuracy using only pure-component diffusivity and isotherm data.

Figure 8 shows the experimental permeation fluxes for a CO_2/CH_4 mixture campaign in which the total upstream pressure was maintained constant at 3.53 MPa and the proportions of the two species was varied. Also in this case, the M−S model (eq 3) yields results in good agreement with the experiment.

Figure 9 shows the experimentally determined permeation selectivity α_{perm} defined by

$$\alpha_{perm} = \frac{N_1/N_2}{f_{1,up}/f_{2,up}} \tag{13}$$

for (a) CO_2/CH_4, (b) CO_2/N_2, and (c) N_2/CH_4 mixtures. In all three cases, the measured α_{perm} decreases with increasing values of the upstream total pressure $f_{up} = f_{1,up} + f_{2,up}$. The reason for this is to be found in the loading dependence of the transport coefficients; cf. Figure 3b. For both CO_2/CH_4 and CO_2/N_2 mixtures, the transport coefficient of CO_2 increases less sharply with loading than that of CH_4 and N_2; this causes the selectivity α_{perm} to decrease with increasing loading on the upstream face. For the N_2/CH_4 mixture, the reduction in α_{perm} with increasing f_{up} is caused by the fact that the diffusivity of CH_4 increases more sharply with loading than that of N_2.

For all three mixtures, integration of eq 3 provides a very good estimate of the measured α_{perm}; see the calculations indicated by the continuous solid lines. Inclusion of the binary exchange coefficient $Đ_{12}$, estimated using eq 2, in the M−S eq 1, will have the effect of slowing down the "faster" molecules while concomitantly speeding-up the "tardier" molecules. These predictions are shown by the dashed lines in Figure 9 parts a, b, and c; for all three mixtures, this leads to a significantly poorer match with the experiments. For CO_2/CH_4 and N_2/CH_4 mixtures, allowance of a finite binary exchange coefficient $Đ_{12}$ predicts a significantly *lower* α_{perm} than in the experiments because of the slowing-down of the more mobile CO_2, or N_2, and concomitant speeding-up of the tardy CH_4 in both these cases. For the CO_2/N_2 mixture, inclusion of $Đ_{12}$ leads to a significantly *higher* value of α_{perm} than that found experimentally; this is because of the slowing-down of the relatively more mobile N_2 and the speeding-up of CO_2.

The conclusion to be drawn from the results presented in Figures 7−9 is that intercage hopping of molecules within SAPO-34 occurs independent of each other and validates the use of the simplified M−S eq 3. There is no perceptible slowing-down or speeding-up process. The window size of SAPO-34 is of the order of 3.8 Å, and only one molecule can pass through the window at a time; this can also be visualized in the snapshots in Figure 10 obtained from Grand Canonical Monte Carlo simulations of the CO_2 and CH_4 in SAPO-34. The intercage hopping of molecules between cages is uncorrelated, and the binary exchange coefficient $Đ_{12}$ has a large value.

For CO_2/CH_4 mixture permeation in DDR, the situation can be expected to be analogous to that of SAPO-34.[10] This is confirmed by an analysis of the published experimental data of Tomita et al.[7] for CO_2/CH_4 mixture permeation across a DDR membrane at 300 and 373 K; the information has been presented in Appendix C of the Supporting Information. Appendix C also confirms the ability of eq 3 to provide a reasonable prediction

of mixture diffusion at a various temperatures across the SAPO-34 membrane using the earlier set of experiments of Li et al.[8]

5. Conclusions

The following conclusions can be drawn from the results presented in this paper.

(1) The M−S diffusivities $Đ_i$ of CO_2, CH_4, and N_2 in SAPO-34 are all loading dependent. The larger the diameter of the molecule, the stronger is the loading dependence, characterized by the Reed and Ehrlich parameter ϕ_i.

(2) A unary permeation model incorporating the Reed−Ehrlich description of the $Đ_i - q_i$ dependence provides a good description of the experimental unary permeation data for CO_2, CH_4, and N_2.

(3) Binary CO_2/CH_4, CO_2/N_2, N_2/CH_4 mixture permeation in SAPO-34 is best modeled by the M−S eq 3, wherein the intercage hopping of molecules is taken to be independent of one another. This conclusion also holds for mixture permeation in other cage-type zeolites with narrow windows, such as DDR. Mixture permeation can be predicted very well using only pure-component transport and isotherm data.

Acknowledgment

The Boulder group gratefully acknowledges support by the Shell Global Solutions. R.K. acknowledges the grant of a TOP subsidy from The Netherlands Foundation for Fundamental Research (NWO-CW) for intensification of reactors and NWO/NCF for provision of high performance computing resources. Dr. J. M. van Baten provided valuable assistance in MC and MD simulations. Financial support from ExxonMobil Research and Engineering allowed R.K. to spend a short sabbatical stay at Boulder.

Supporting Information Available: Appendix A includes details of membrane synthesis, characterization, and measurement procedures along with the experimental data. Appendix B is a short note explaining the advantages of using Ruthven's statistical isotherm. Appendix C presents an analysis of the published mixture permeation data in the older version of the SAPO-34 membrane and in DDR. This material is available free of charge via the Internet at http://pubs.acs.org.

Nomenclature

b_i = constant in eq 4, Pa^{-1}
$Đ_i$ = Maxwell−Stefan diffusivity of species i, $m^2\ s^{-1}$
$Đ_i(0)$ = zero-loading M−S diffusivity of species i, $m^2\ s^{-1}$
$Đ_{12}$ = binary exchange diffusivity, $m^2\ s^{-1}$
DF_i = driving force for transport across membrane, mol kg^{-1}
f_i = fugacity of species i, Pa
MDF_i = modified driving force for transport across membrane, mol kg^{-1}
N_i = molar flux of species i across membrane, mol $m^{-2}\ s^{-1}$
q_i = molar loading, mol kg^{-1}
$q_{i,sat}$ = saturation loading, mol kg^{-1}
R = gas constant, 8.314 J $mol^{-1}\ K^{-1}$
T = absolute temperature, K
z = coordination number, dimensionless

Greek Letters

α_{perm} = permeation selectivity, dimensionless
β_i = Reed−Ehrlich parameter, dimensionless
ϕ_i = Reed−Ehrlich parameter, dimensionless
δ = thickness of zeolite membrane, m
ϵ_i = Reed−Ehrlich parameter, dimensionless
θ_i = fractional occupancy of component i, dimensionless
μ_i = molar chemical potential, J mol^{-1}
ρ = density of zeolite, kg m^{-3}
Ω_i = saturation capacity, molecules $cage^{-1}$

Subscripts

down = referring to downstream conditions
sat = referring to saturation conditions
up = referring to upstream conditions

Literature Cited

(1) Kapteijn, F.; Moulijn, J. A.; Krishna, R. The generalized Maxwell−Stefan model for diffusion in zeolites: Sorbate molecules with different saturation loadings. *Chem. Eng. Sci.* **2000**, *55*, 2923−2930.

(2) Krishna, R.; van Baten, J. M. Diffusion of alkane mixtures in zeolites. Validating the Maxwell−Stefan formulation using MD simulations. *J. Phys. Chem. B* **2005**, *109*, 6386−6396.

(3) Krishna, R.; van Baten, J. M. Describing binary mixture diffusion in carbon nanotubes with the Maxwell−Stefan equations. An investigation using molecular dynamics simulations. *Ind. Eng. Chem. Res.* **2006**, *45*, 2084−2093.

(4) van de Graaf, J. M.; Kapteijn, F.; Moulijn, J. A. Modeling permeation of binary mixtures through zeolite membranes. *AIChE J.* **1999**, *45*, 497−511.

(5) Millot, B.; Methivier, A.; Jobic, H.; Moueddeb, H.; Bee, M. Diffusion of isobutane in ZSM-5 zeolite: A comparison of quasi-elastic neutron scattering and supported membrane results. *J. Phys. Chem. B* **1999**, *103*, 1096−1101.

(6) Krishna, R.; Baur, R. Modelling issues in zeolite based separation processes. *Sep. Purif. Technol.* **2003**, *33*, 213−254.

(7) Tomita, T.; Nakayama, K.; Sakai, H. Gas separation characteristics of DDR type zeolite membrane. *Microporous Mesoporous Mater.* **2004**, *68*, 71−75.

(8) Li, S.; Martinek, J. G.; Falconer, J. L.; Noble, R. D.; Gardner, T. Q. High-Pressure CO_2/CH_4 separation using SAPO-34 membranes. *Ind. Eng. Chem. Res.* **2005**, *44*, 3220−3228.

(9) Zhu, W.; Hrabanek, P.; Gora, L.; Kapteijn, F.; Moulijn, J. A. Role of Adsorption in the Permeation of CH_4 and CO_2 through a Silicalite-1 Membrane. *Ind. Eng. Chem. Res.* **2006**, *45*, 767−776.

(10) Krishna, R.; van Baten, J. M.; García-Pérez, E.; Calero, S. Incorporating the loading dependence of the Maxwell−Stefan diffusivity in the modeling of CH_4 and CO_2 permeation across zeolite membranes. *Ind. Eng. Chem. Res.* **2007**, *46*, in press; DOI: 10.1021/ie060693d.

(11) Krishna, R.; van Baten, J. M.; García-Pérez, E.; Calero, S. Diffusion of CH_4 and CO_2 in MFI, CHA and DDR zeolites. *Chem. Phys. Lett.* **2006**, *429*, 219−224.

(12) Ruthven, D. M. *Principles of Adsorption and Adsorption Processes*; John Wiley: New York, 1984.

(13) Mäder, U. K.; Berman, R. G. An equation of state for carbon dioxide to high pressure and temperature. *Am. Mineral.* **1991**, *76*, 1547−1559.

(14) Golden, T. C.; Sircar, S. Gas-Adsorption on Silicalite. *J. Colloid Interface Sci.* **1994**, *162*, 182−188.

(15) Reed, D. A.; Ehrlich, G. Surface diffusion, atomic jump rates and thermodynamics. *Surf. Sci.* **1981**, *102*, 588−609.

(16) Krishna, R.; Paschek, D.; Baur, R. Modelling the occupancy dependence of diffusivities in zeolites. *Microporous Mesoporous Mater.* **2004**, *76*, 233−246.

(17) Dubbeldam, D.; Calero, S.; Vlugt, T. J. H.; Krishna, R.; Maesen, T. L. M.; Smit, B. United Atom Forcefield for Alkanes in Nanoporous Materials. *J. Phys. Chem. B* **2004**, *108*, 12301−12313.

(18) Makrodimitris, K.; Papadopoulos, G. K.; Theodorou, D. N. Prediction of permeation properties of CO_2 and N_2 through silicalite via molecular simulations. *J. Phys. Chem. B* **2001**, *105*, 777−788.

(19) Beerdsen, E.; Dubbeldam, D.; Smit, B. Molecular Understanding of Diffusion in Confinment. *Phys. Rev. Lett.* **2005**, *95*, 164505.

(20) Beerdsen, E.; Dubbeldam, D.; Smit, B. Understanding Diffusion in Nanoporous Materials. *Phys. Rev. Lett.* **2006**, *96*, 044501.

(21) Krishna, R.; Baur, R. *Diffusion, Adsorption and Reaction in Zeolites: Modelling and Numerical Issues*; University of Amsterdam: Amsterdam, The Netherlands, 11 Nov, 2004; http://www.science.uva.nl/research/cr/zeolite/.

(22) Myers, A. L.; Prausnitz, J. M. Thermodynamics of mixed gas adsorption. *AIChE J.* **1965**, *11* (1), 121−130.

Received for review August 14, 2006
Revised manuscript received September 25, 2006
Accepted September 26, 2006

IE0610703

Supporting information to accompany:

Modeling permeation of CO_2/CH_4, CO_2/N_2, and N_2/CH_4 mixtures across SAPO-34 membrane with the Maxwell-Stefan equations

Shiguang Li[(1)], John L. Falconer[(1)], Richard D. Noble[(1)], and R. Krishna[(2)]*

[(1)] Department of Chemical and Biological Engineering, University of Colorado

Boulder, CO 80309-0424, U.S.A.

[(2)]Van 't Hoff Institute for Molecular Sciences, University of Amsterdam, Nieuwe Achtergracht 166,

1018 WV Amsterdam, The Netherlands.

Contents:

Appendix A: Experimental Methods and Data

Appendix B: A note on fitting with the statistical isotherm of Ruthven

Appendix C: Analysis of CH_4 - CO_2 mixture permeation data in SAPO-34 (older version) and DDR membranes.

Appendix A: Experimental Methods and Data

1. Experimental Methods

Membrane Synthesis

SAPO-34 membranes were synthesized by seeding on porous stainless steel tubes (0.8-μm pores, Pall Corp.). The detailed synthesis procedure was given elsewhere.[1] Non-porous, stainless steel tubes were welded onto each end of supports. The permeate area was approximately 7.8 cm^2. The synthesis gel composition for SAPO-34 seeds was 1.0 Al_2O_3 : 1.0 P_2O_5 : 0.3 SiO_2 : 1.2 TEAOH : 55 H_2O. This composition is different to that used in our previous published study.[2]

The gel was prepared by stirring H_3PO_4 (85 wt% aqueous solution, Aldrich), $Al(i\text{-}C_3H_7O)_3$ (> 99.99%, Aldrich), and distilled H_2O at room temperature for 12 h. Then the template, tetra-ethyl ammonium hydroxide (TEAOH, 35 wt% aqueous solution, Aldrich), was added and the mixture stirred for 30 min before the colloidal silica sol (Ludox AS40, 40% aqueous solution, Aldrich) was added to the mixture. The solution was sealed, stirred, and aged for approximately 24 h at room temperature. Next, the gel was added to a Teflon-lined autoclave. The hydrothermal synthesis was carried at 493 K for about 24 h. After synthesis, the powder was collected and washed with distilled water at 295 K for three times, and then dried at 373 K in a vacuum oven for 2 h. The powder was calcined at 823 K for 10 h. The heating and cooling rates were 6 K/min. The calcined crystals were used as seeds for membrane preparation.

Before membrane synthesis, the supports were boiled in distilled water for 3 h and dried at 373 K under vacuum for 30 min. The stainless steel tubes were then wrapped with Teflon tape on their outside. The tubes were then treated by rubbing the inside surface of the support tube with dry SAPO-34 particles. The seeded tubes were placed in an autoclave, which was then filled with the synthesis gel that has the same composition as that used for seeds. The hydrothermal synthesis was carried at 493 K for about 24 h. After synthesis, the membrane was washed with distilled water at 295 K and dried at 373

K in a vacuum oven for 2 h. A second synthesis step was applied using the same procedure, but the tube was inverted to obtain a more uniform layer. The membranes were calcined in air at 663 K for 10 h. The heating and cooling rates were 0.6 and 0.9 K/min, respectively.

Characterization

Crystals collected during membrane synthesis were calcined at 823 K for 10 h, and then used in various analyses including adsorption measurements. X-ray diffraction (XRD, Scintag PAD-V diffractometer) confirmed the CHA structure. The chemical composition of the crystals determined by inductively coupled plasma analysis (Varian UltraMass 700 inductively coupled plasma mass spectrometer with a CETAC LXS-200+ laser ablation system) was $(Si_{0.061}Al_{0.483}P_{0.455})O_2$.

Adsorptions were carried out in an Autosorb-1 (Quantachrome Corp. Model AS1-C-VP-RGA) system. Prior to each adsorption experiment, the sample was outgassed in vacuum at 493 K for at least 2 h. Adsorption isotherms for CO_2, CH_4 and N_2 were measured at 295 K. Nitrogen adsorption was performed at 77 K to determine the BET surface area and micropore volume. The SAPO-34 zeolite had a BET surface area of 500 m^2/g and a micropore volume of 0.26 cm^3/g.

Unary and binary Permeation

Single-gas, and binary CO_2/CH_4, CO_2/N_2, and N_2/CH_4 mixture permeations were measured in the flow system described previously;[2] the system was modified to operate up to 7.2 MPa pressure. The membrane was mounted in a stainless steel module and sealed at each end with silicone o-rings. The pressure on each side of the membrane was independently controlled. Unary and mixture permeations were investigated as functions of feed pressure while maintaining a constant permeate pressure of 84 kPa. For CO_2/CH_4 mixture separation, a pre-mixed gas (Airgas) was used. For CO_2/N_2, and N_2/CH_4 mixture separations mass flow controllers were used to mix pure gases in specified ratios. Fluxes were measured using a soap film bubble flow meter. The system was leak checked by replacing the membrane with a solid stainless steel tube. The leak rate for a 7-MPa pressure drop across the O-ring was less than 0.01% of the measured CH_4 flux for a 50/50 mixture at the same pressure drop across a membrane.

Figure 1 shows a schematic of the membrane set-up.The compositions of the feed, retentate, and permeate streams were measured online using a SRI 8610 C GC gas chromatograph equipped with a thermal conductivity detector and HAYESEP-D column (Alltech). The oven, injector, and detector temperatures were all kept at 423 K.

2. Permeation data

The experimental data for unary permeation of CO_2, CH_4 and N_2 are presented in Tables 1, 2 and 3. The binary permeation data for CO_2/CH_4, CO_2/N_2, and N_2/CH_4 mixtures are summarized in Tables 4, 5 and 6. The feed gas composition for the CO_2/CH_4 and N_2/CH_4 mixtures was precisely equimolar. For the CO_2/N_2 mixtures the feed gas composition was in the proportion 52.7% and 47.3%. The gas phase compositions of the retentate (upstream) and permeate (downstream) compartments were also measured and on this basis the partial pressures on both compartments were determined. The *average* (logarithmic mean) values of the upstream partial pressures, $f_{i,up}$, are reported in the second and third columns of Tables 4, 5 and 6 were used. For purposes of model calculations to compare with experiments, the precise partial pressures as specified in the second and third columns of Tables 4, 5 and 6 were used. The permeation selectivity α_{perm} defined by

$$\alpha_{perm} = \frac{N_1/N_2}{f_{1,up}/f_{2,up}} \qquad (1)$$

are presented in the last column of Tables 4, 5 and 6.

For plotting purposes the total upstream pressures, listed in the first column in Tables 4, 5 and 6 are employed on the x-axis in the main text of this paper.

For the binary CO_2/CH_4 mixture an additional permeation campaign was carried out in which the total upstream pressure was maintained constant at 3.53 MPa, and the proportions of CO_2 and CH_4 in the upstream compartment were varied. The data is summarized in Table 7.

3. Literature cited

(1) Li, S.; Falconer, J. L.; Noble, R. D., Improved SAPO-34 Membranes for CO_2/CH_4 Separations, *Adv. Mater.* **2006**, Manuscript in Press, DOI: 10.1002/adma.200601147.

(2) Li, S.; Martinek, J. G.; Falconer, J. L.; Noble, R. D.; Gardner, T. Q., High-Pressure CO_2/CH_4 separation using SAPO-34 membranes, *Ind. Eng. Chem. Res.* **2005**, *44*, 3220-3228.

Table 1. Unary CO_2 permeation data.

Upstream pressure, $f_{i,up}$	Downstream pressure, $f_{i,down}$	CO_2 flux, N_i
0.43	0.084	0.083
0.77	0.084	0.129
1.46	0.084	0.186
2.15	0.084	0.215
2.84	0.084	0.238
3.53	0.084	0.253
4.22	0.084	0.266
4.91	0.084	0.278
5.60	0.084	0.290

$f_{i,up}$ and $f_{i,down}$ have the units MPa, N_i are expressed in mol m^{-2} s^{-1}

Table 2. Unary CH_4 permeation data.

Upstream pressure, $f_{i,up}$	Downstream pressure, $f_{i,down}$	CH_4 flux, N_i
0.43	0.084	0.0012
0.77	0.084	0.0025
1.46	0.084	0.0048
2.15	0.084	0.0072
2.84	0.084	0.0093
3.53	0.084	0.0111
4.22	0.084	0.0133
4.91	0.084	0.0154
5.60	0.084	0.0175
6.29	0.084	0.0197
7.08	0.084	0.0220

$f_{i,up}$ and $f_{i,down}$ have the units MPa, N_i are expressed in mol m^{-2} s^{-1}

Table 3. Unary N_2 permeation data.

Upstream pressure. $f_{i,up}$	Downstream pressure, $f_{i,down}$	N_2 flux, N_i
0.43	0.084	0.009
0.77	0.084	0.017
1.46	0.084	0.027
2.15	0.084	0.041
2.84	0.084	0.053
3.53	0.084	0.065
4.22	0.084	0.077
4.91	0.084	0.087
5.60	0.084	0.098
6.29	0.084	0.108
6.98	0.084	0.119

$f_{i,up}$ and $f_{i,down}$ have the units MPa, N_i are expressed in mol m^{-2} s^{-1}

Table 4. Binary CO_2-CH_4 permeation data. The feed composition was 50% : 50%.

Total upstream pressure f_{up}	CO_2 upstream partial pressure $f_{1,up}$	CH_4 upstream partial pressure $f_{2,up}$	CO_2 downstream partial pressure $f_{1,down}$	CH_4 downstream partial pressure $f_{2,down}$	CO_2 flux N_1	CH_4 flux N_2	Permeation selectivity, α_{perm}
0.77	0.37	0.40	0.083	0.0013	0.064	0.0010	68.1
1.46	0.69	0.77	0.083	0.0014	0.102	0.0017	68.2
2.50	1.14	1.35	0.083	0.0014	0.140	0.0024	69.4
3.88	1.72	2.14	0.082	0.0017	0.171	0.0035	61.5
5.26	2.27	2.95	0.082	0.0018	0.196	0.0044	58.1
6.70	2.82	3.83	0.082	0.0020	0.221	0.0055	54.4
7.19	3.00	4.13	0.082	0.0021	0.228	0.0059	53.0

$f_{i,up}$ and $f_{i,down}$ have the units MPa, N_i are expressed in mol m^{-2} s^{-1}

Table 5. Binary CO_2-N_2 permeation data. The feed composition was 52.7% : 47.3%.

Total upstream pressure f_{up}	CO_2 upstream partial pressure $f_{1,up}$	N_2 upstream partial pressure $f_{2,up}$	CO_2 downstream partial pressure $f_{1,down}$	N_2 downstream partial pressure $f_{2,down}$	CO_2 flux N_1	N_2 flux N_2	Permeation selectivity, α_{perm}
0.77	0.39	0.38	0.079	0.005	0.065	0.0037	16.8
1.46	0.72	0.74	0.080	0.004	0.108	0.0059	18.6
2.15	1.04	1.11	0.079	0.005	0.136	0.0091	16.1
2.83	1.35	1.48	0.079	0.005	0.154	0.0107	15.8
3.52	1.66	1.86	0.078	0.006	0.168	0.0122	15.5

$f_{i,up}$ and $f_{i,down}$ have the units MPa, N_i are expressed in mol m^{-2} s^{-1}

Table 6. Binary N_2 –CH_4 permeation data. The feed composition was 50% : 50%.

Total upstream pressure f_{up}	N_2 upstream partial pressure $f_{1,up}$	CH_4 upstream partial pressure $f_{2,up}$	N_2 downstream partial pressure $f_{1,down}$	CH_4 downstream partial pressure $f_{2,down}$	N_2 flux N_1	CH_4 flux N_2	Permeation selectivity, α_{perm}
0.773	0.386	0.388	0.079	0.005	0.065	0.0037	4.98
1.463	0.728	0.735	0.080	0.004	0.108	0.0059	4.52
2.152	1.069	1.084	0.079	0.005	0.136	0.0091	4.19
2.842	1.409	1.433	0.079	0.005	0.154	0.0107	4.00
3.531	1.748	1.783	0.078	0.006	0.168	0.0122	3.81

$f_{i,up}$ and $f_{i,down}$ have the units MPa, N_i are expressed in mol m^{-2} s^{-1}

Table 7. Binary CO_2-CH_4 permeation data with varying compositions at constant upstream total pressure = 3.53 MPa.

Mole fraction of CO_2 in upstream compartment	CO_2 upstream partial pressure $f_{1,up}$	CH_4 upstream partial pressure $f_{2,up}$	CO_2 downstream partial pressure $f_{1,down}$	CH_4 downstream partial pressure $f_{2,down}$	CO_2 flux N_1	CH_4 flux N_2
0.05	0.16	3.37	0.054	0.0304	0.017	0.00952
0.12	0.43	3.09	0.073	0.0109	0.045	0.00676
0.35	1.24	2.29	0.082	0.0025	0.131	0.00400
0.45	1.59	1.93	0.082	0.0016	0.163	0.00309
0.59	2.09	1.44	0.083	0.0009	0.193	0.00198
0.83	2.92	0.60	0.084	0.0002	0.240	0.00065

$f_{i,up}$ and $f_{i,down}$ have the units MPa, N_i are expressed in mol m^{-2} s^{-1}

4. Captions for Figures

Figure 1. Schematic of membrane set-up.

Figure 1

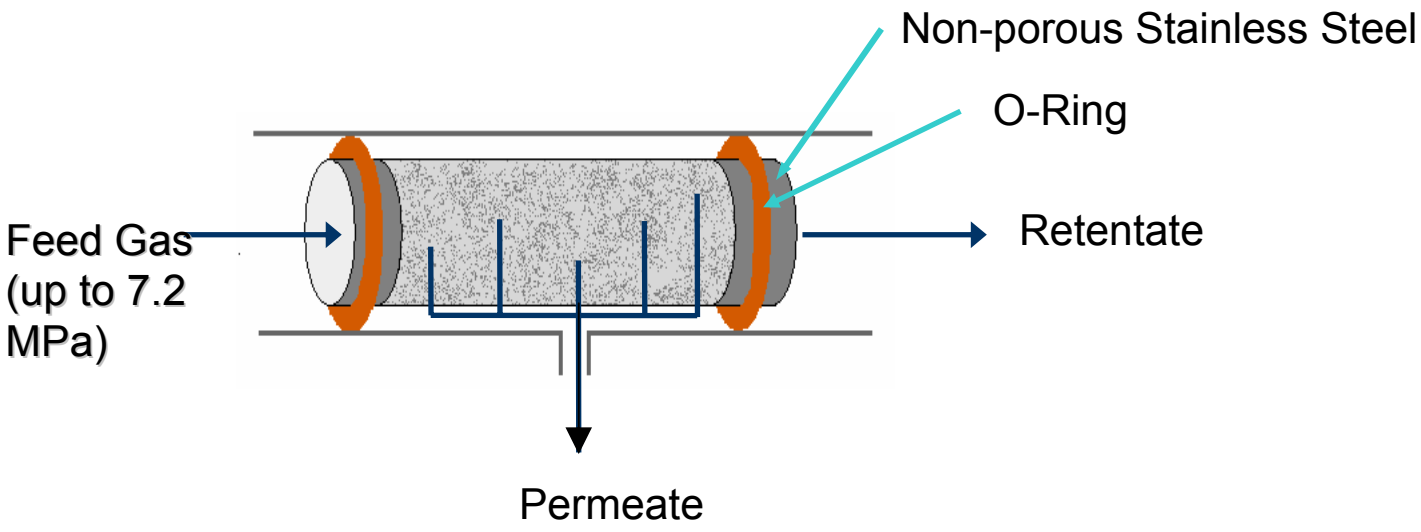
Non-porous Stainless Steel
O-Ring
Feed Gas
(up to 7.2
MPa)
Retentate
Permeate

Appendix B: A note on fitting with the statistical isotherm of Ruthven

In order to establish the advantages of the use of Ruthven's statistical isotherm

$$q_i = \frac{q_{i,sat}}{\Omega_i} \frac{b_i f_i + \sum_{m=2}^{\Omega_i} \frac{(b_i f_i)^m}{(m-1)!} \left[\frac{1 - \frac{m}{\Omega_i + 1}}{1 - \frac{1}{\Omega_i + 1}} \right]^m}{1 + b_i f_i + \sum_{m=2}^{\Omega_i} \frac{(b_i f_i)^m}{(m)!} \left[\frac{1 - \frac{m}{\Omega_i + 1}}{1 - \frac{1}{\Omega_i + 1}} \right]^m} \qquad (1)$$

for fitting purposes let us consider the GCMC simulations for CO_2 isotherms in CHA at 300 K reported by Krishna et al.[1] In eq (1) q_i represents the loading in mol kg^{-1}, $q_{i,sat}$ is the saturation loading, and Ω_i is maximum capacity in molecules per cage.

For the CHA (all-silica) used in the simulations

$$q_{i,sat} = 1.397\Omega_i \qquad (2)$$

This data is plotted in Figure 1. For good representation of this data, Krishna et al.[1] resorted to a 3-site Langmuir fit, with a total of 6 parameters to accurately represent the data. Fitting of eq (1) taking $\Omega = 7$ molecules per cage is shown in Figure 1 with the continuous solid line. A good fit is obtained with only two parameters, b_i and Ω.

The GCMC simulation results for N_2 in CHA at 300 K are shown in Figure 2. A good fit with eq (1) is obtained taking $\Omega = 6$ molecules per cage.

For DDR too there are advantages of using eq (1), as shown by the GCMC simulation results for adsorption of CO_2 at 300 K; see Figure 3. Note that for all-silica DDR

$$q_{i,sat} = 0.832\Omega_i \qquad (3)$$

The data can be fitted adequately taking Ω = 6 molecules per cage. Krishna et al.[1] used a 3-site Langmuir fit, with a total of 6 parameters to accurately represent the data.

For fitting of experimental data restricted to relatively low pressure ranges, the advantages of using eq (1) is particularly evident. There is usually not enough data to warrant a multi-site Langmuir fit.

References

(1) Krishna, R.; van Baten, J. M.; García-Pérez, E.; Calero, S., Incorporating the loading dependence of the Maxwell-Stefan diffusivity in the modeling of CH_4 and CO_2 permeation across zeolite membranes, *Ind. Eng. Chem. Res.* **2007**, *46*, Manuscript in press, DOI: 10.1021/ie060693d.

1. Captions for Figures

Figure 1. Pure component isotherm data of CO_2 in CHA at 300 K obtained from GCMC simulations[1] along with fit using eq (1), denoted by the continuous solid lines.

Figure 2. Pure component isotherm data of N_2 in CHA at 300 K obtained from GCMC simulations along with fit using eq (1), denoted by the continuous solid lines.

Figure 3. Pure component isotherm data of CO_2 in DDR at 300 K obtained from GCMC simulations[1] along with fit using eq (1), denoted by the continuous solid lines.

Figure 1

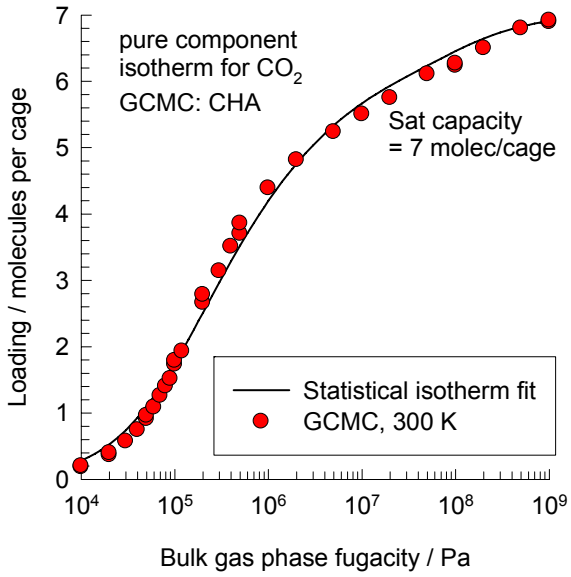
pure component
isotherm for CO_2
GCMC: CHA
Sat capacity
= 7 molec/cage
Statistical isotherm fit
GCMC, 300 K
Loading / molecules per cage
Bulk gas phase fugacity / Pa
0
1
2
3
4
5
6
7
10^4
10^5
10^6
10^7
10^8
10^9

Figure 2

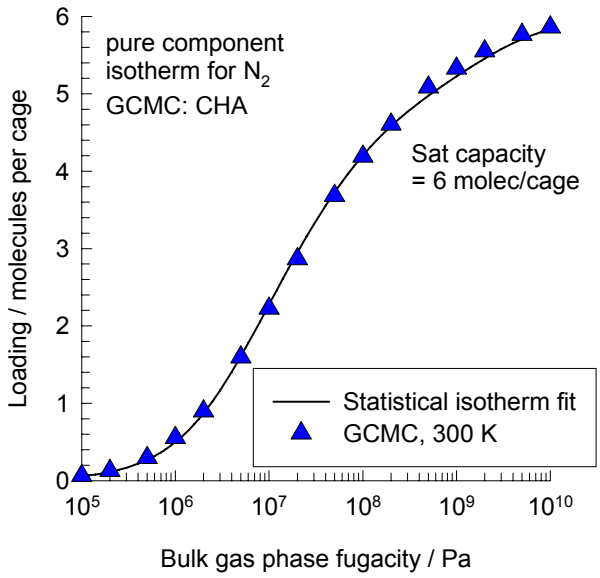
pure component
isotherm for N_2
GCMC: CHA
Sat capacity
= 6 molec/cage
Statistical isotherm fit
GCMC, 300 K
Loading / molecules per cage
Bulk gas phase fugacity / Pa
0
1
2
3
4
5
6
10^5
10^6
10^7
10^8
10^9
10^{10}

Figure 3

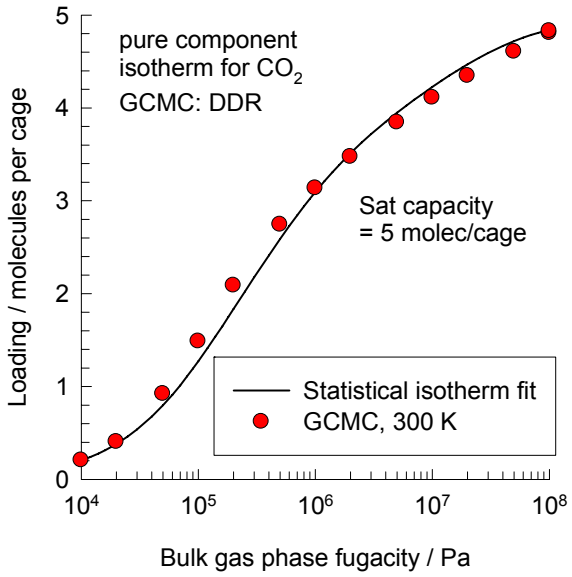
pure component
isotherm for CO_2
GCMC: DDR
Sat capacity
= 5 molec/cage
Statistical isotherm fit
GCMC, 300 K
Loading / molecules per cage
Bulk gas phase fugacity / Pa
0
1
2
3
4
5
10^4
10^5
10^6
10^7
10^8

Appendix C: CH_4 - CO_2 mixture permeation data analysis in SAPO-34 (older version) and DDR membranes

1. CO_2 - CH_4 mixture permeation through SAPO-34 membrane

We re-analyse the CO_2 - CH_4 50-50 mixture permeation experiments of Li et al.[1] The membrane used in this previous study was synthesized using a different procedure and offered a lower permeation selectivity; a comparison of the performances of the older version of the membrane[1] and the current one, described in detail in Appendix A of Supporting Information, is presented in Figure 1.

We would like to demonstrate that the separation selectivity of the older version can *also* be modeled adequately using the M-S equations, ignoring the binary exchange parameter $Đ_{12}$

$$N_i = -\rho Đ_i \frac{q_i}{RT}\frac{d\mu_i}{dz}; \quad i = 1,...n \tag{1}$$

This model is termed the M-S mixture model.

The detailed analysis of unary permeation data of CO_2 and CH_4 at various temperatures 295 K, 333 K, 373 K, 423 K and 473 K has been presented in our earlier work.[2] In this previous study the transport coefficient of CO_2 was found to be nearly loading independent. In analyzing the permeation data, the isotherms were calculated using Grand Canonical Monte Carlo (GCMC) simulations[2] with all-silica CHA. These simulation results are assumed to be valid also for SAPO-34; this assumption has been tested earlier to be valid.[2] The 3-site Langmuir model parameters are listed in Table 1. The Reed and

Ehrlich parameters listed in Table 2. The fitted value of the transport coefficients are listed in Table 3 for various temperatures.

Figure 2 compares the mixture permeation selectivity at 295 K with SAPO-34 (obtained with previous membrane of Li et al.[1]) with predictions of the M-S mixture model. In the model calculations eq (1) was integrated across the membrane using the numerical procedure described in earlier work.[3, 4] Also shown is the sorption selectivity calculated using the IAST.[5] The experimental trend in the permeation selectivity is reasonably well reproduced by eq (1). The clue to good predictions appears to lie in the proper fitting of the transport coefficients.

We turn to prediction of permeation selectivity as a function of temperature. The temperature dependence of the 3-site Langmuir parameters, reported in Table 1 are fitted as described in Table 4. The temperature dependence of the transport coefficients as listed in Table 3 for SAPO-34 are fitted using the expressions given in Table 5. Figure 3a compares the values in Table 3 with the fitted expressions in Table 5.

With the information given in Table 4 and Table 5 we can calculate the permeation selectivity as a function of temperature for fixed pressures upstream and downstream of the membrane. Figure 3b compare of mixture permeation selectivity obtained by Li et al.[1] in their experiments with a pressure drop of 3 MPa across the membrane with predictions of the M-S mixture model. The agreement between experiment and model is good over the entire temperature range.

2. CH_4 - CO_2 mixture permeation through DDR membrane

The re-analysis of the CH_4 permeation experiments of Tomita et al.[6] in DDR The detailed analysis of unary permeation data of CO_2 and CH_4 at temperatures 300 K and 373 K has been presented in our earlier work.[2] The 3-site Langmuir model parameters are listed in Table 1. The Reed and Ehrlich parameters listed in Table 2. The fitted value of the transport coefficients are listed in Table 3 for the two temperatures. Figure 4 compares the mixture permeation selectivity at (a) 300 K, and (b) 373 K with DDR membrane by Tomita et al.[6] with predictions of the M-S mixture model. Also shown is the

sorption selectivity calculated using the IAST.[5] The agreement between experiment and model is reasonably good for both temperatures.

3. Literature cited

(1) Li, S.; Martinek, J. G.; Falconer, J. L.; Noble, R. D.; Gardner, T. Q., High-Pressure CO_2/CH_4 separation using SAPO-34 membranes, *Ind. Eng. Chem. Res.* **2005**, *44*, 3220-3228.

(2) Krishna, R.; van Baten, J. M.; García-Pérez, E.; Calero, S., Incorporating the loading dependence of the Maxwell-Stefan diffusivity in the modeling of CH_4 and CO_2 permeation across zeolite membranes, *Ind. Eng. Chem. Res.* **2007**, *46*, Manuscript in press, DOI: 10.1021/ie060693d.

(3) Krishna, R.; Baur, R., Modelling issues in zeolite based separation processes, *Sep. Purif. Technol.* **2003**, *33*, 213-254.

(4) Krishna, R.; Baur, R., Diffusion, Adsorption and Reaction in Zeolites: Modelling and Numerical Issues, http://ct-cr4.chem.uva.nl/zeolite/, University of Amsterdam, Amsterdam, 11 November 2004.

(5) Myers, A. L.; Prausnitz, J. M., Thermodynamics of mixed gas adsorption, *A.I.Ch.E.J.* **1965**, *11*, 121-130.

(6) Tomita, T.; Nakayama, K.; Sakai, H., Gas separation characteristics of DDR type zeolite membrane, *Microporous Mesoporous Mater.* **2004**, *68*, 71-75.

Table 1. Three-site Langmuir parameters for CH_4 and CO_2 in CHA (taken to be equivalent to SAPO-34 as regards sorption data) and DDR. The saturation capacity q_{sat} has the units of mol kg^{-1}. The Langmuir parameters b_i, have the units of Pa^{-1}.

Zeolite	Molecule, Temperature	Three-Site Langmuir parameters					
		$b_{i,A}$	$q_{i,sat,A}$	$b_{i,B}$	$q_{i,sat,B}$	$b_{i,C}$	$q_{i,sat,C}$
CHA	CH_4, 300 K	1.72×10^{-6}	2.77	2.7×10^{-8}	4.16	9.0×10^{-10}	1.39
CHA	CH_4, 333 K	9.0×10^{-7}	2.77	1.4×10^{-8}	4.16	4.0×10^{-10}	1.39
CHA	CH_4, 373 K	4.53×10^{-7}	2.77	7.4×10^{-9}	4.16	2.1×10^{-10}	1.39
DDR	CH_4, 373 K	3.5×10^{-6}	1.66	1.45×10^{-8}	1.66	2.7×10^{-11}	0.83
CHA	CO_2, 300 K	5.21×10^{-6}	6.93	1.02×10^{-7}	1.73	1.17×10^{-9}	1.73
CHA	CO_2, 373 K	5.24×10^{-7}	6.93	4.36×10^{-9}	1.73	1.09×10^{-10}	1.73
CHA	CO_2, 423 K	1.88×10^{-7}	6.93	1.28×10^{-9}	1.73	3.84×10^{-11}	1.73
CHA	CO_2, 473 K	1×10^{-7}	6.93	4.84×10^{-10}	1.73	1.6×10^{-11}	1.73
DDR	CO_2, 373 K	7.5×10^{-6}	1.66	2.0×10^{-6}	1.66	1.2×10^{-8}	1.25

Table 2. Reed-Ehrlich parameters.

Zeolite	Molecule	Saturation capacity, $q_{i,sat}$ / mol/kg	Reed-Ehrlich model parameters	
			z	ϕ_i
CHA	CH_4	8.32	6	$3.2\exp(-0.7\theta)$
DDR	CH_4	4.16	6	$6\exp(-0.2\theta)$

Table 3. Fitted values of Transport Coefficients $\rho Đ_i(0)/\delta$ with units of kg m^{-2} s^{-1}.

Zeolite	Molecule	Temperature	$\rho Đ_i(0)/\delta$
SAPO-34	CH_4	295 K	1.4×10^{-3}
SAPO-34	CH_4	333 K	2.3×10^{-3}
SAPO-34	CH_4	373 K	4.5×10^{-3}
DDR	CH_4	300 K	1.84×10^{-5}
DDR	CH_4	373 K	8.36×10^{-5}
SAPO-34	CO_2	295 K	1.54×10^{-2}
SAPO-34	CO_2	373 K	4.45×10^{-2}
SAPO-34	CO_2	423 K	7.85×10^{-2}
SAPO-34	CO_2	473 K	10.03×10^{-2}
DDR	CO_2	300 K	10.31×10^{-5}
DDR	CO_2	373 K	16.83×10^{-5}

Table 4. Temperature dependent 3-site Langmuir parameters for all-silica CHA. These parameters were obtained by carrying out GCMC simulations at various temperatures. This isotherm data is assumed to be valid also for SAPO-34.

For CO_2:

$$b_1 = 6.5\times10^{-11}\exp(\frac{3360}{T}); \quad q_{1,sat} = 6.93 \text{ mol/kg}$$

$$b_2 = 4.12\times10^{-14}\exp(\frac{4350}{T}); \quad q_{2,sat} = 1.73 \text{ mol/kg}$$

$$b_3 = 1.2\times10^{-14}\exp(\frac{3400}{T}); \quad q_{3,sat} = 1.73 \text{ mol/kg}$$

For CH_4:

$$b_1 = 2.44\times10^{-9}\exp(\frac{1960}{T}); \quad q_{1,sat} = 2.77 \text{ mol/kg}$$

$$b_2 = 3.02\times10^{-11}\exp(\frac{2050}{T}); \quad q_{2,sat} = 4.16 \text{ mol/kg}$$

$$b_3 = 2.9\times10^{-13}\exp(\frac{2420}{T}); \quad q_{3,sat} = 1.39 \text{ mol/kg}$$

Table 5. Temperature dependent transport coefficients for SAPO-34.

For CO_2:

$$\frac{\rho Đ_1}{\delta} = \frac{\rho Đ_1(0)}{\delta} = 2.55\exp(-\frac{1504}{T})$$

For CH_4:

$$\frac{\rho Đ_2(0)}{\delta} = 0.3426\exp(-\frac{1635}{T})$$

4. Captions for Figures

Figure 1. Comparison of the mixture permeation selectivity offered by the SAPO-34 membrane used by Li et al.[1] with that presented in current work.

Figure 2. Comparison of mixture permeation selectivity at 295 K with SAPO-34 (obtained with previous membrane of Li et al.[1]) with predictions of the M-S mixture model. Also shown is the sorption selectivity calculated using the IAST.[5]

Figure 3. (a) Temperature dependence of the transport coefficients in SAPO-34 membrane (obtained with previous membrane of Li et al.[1]). (b) Comparison of mixture permeation selectivity at 295 K with SAPO-34 (obtained with previous membrane of Li et al.[1]) with predictions of the M-S mixture model. For the prediction purposes the expressions given in Table 4 and Table 5 are used.

Figure 4. Comparison of mixture permeation selectivity at (a) 300 K, and (b) 373 K with DDR membrane by Tomita et al.[6] with predictions of the M-S mixture model. Also shown is the sorption selectivity calculated using the IAST.[5]

Figure 1

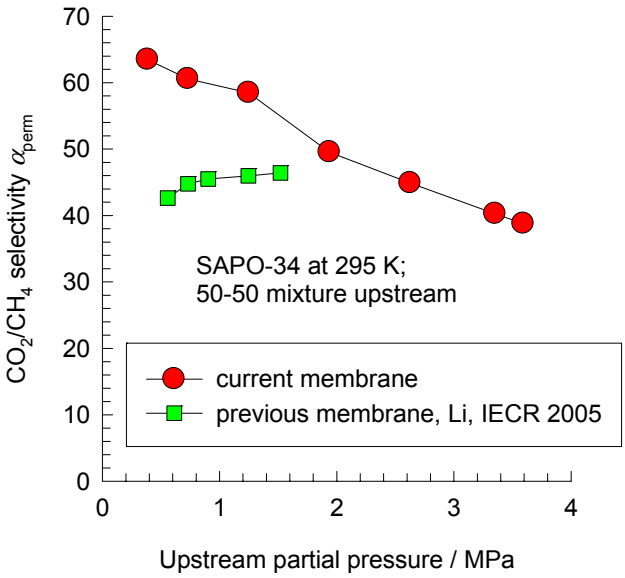
70
60
50
40
30
20
10
0
0
1
2
3
4
CO_2/CH_4 selectivity α_{perm}
Upstream partial pressure / MPa
SAPO-34 at 295 K;
50-50 mixture upstream
current membrane
previous membrane, Li, IECR 2005

Figure 2

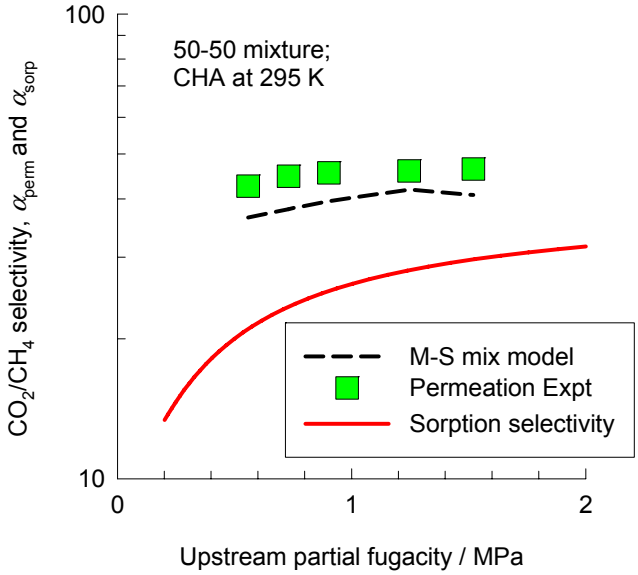
100
10
0
1
2
50-50 mixture;
CHA at 295 K
M-S mix model
Permeation Expt
Sorption selectivity
CO2/CH4 selectivity, αperm and αsorp
Upstream partial fugacity / MPa

Figure 3

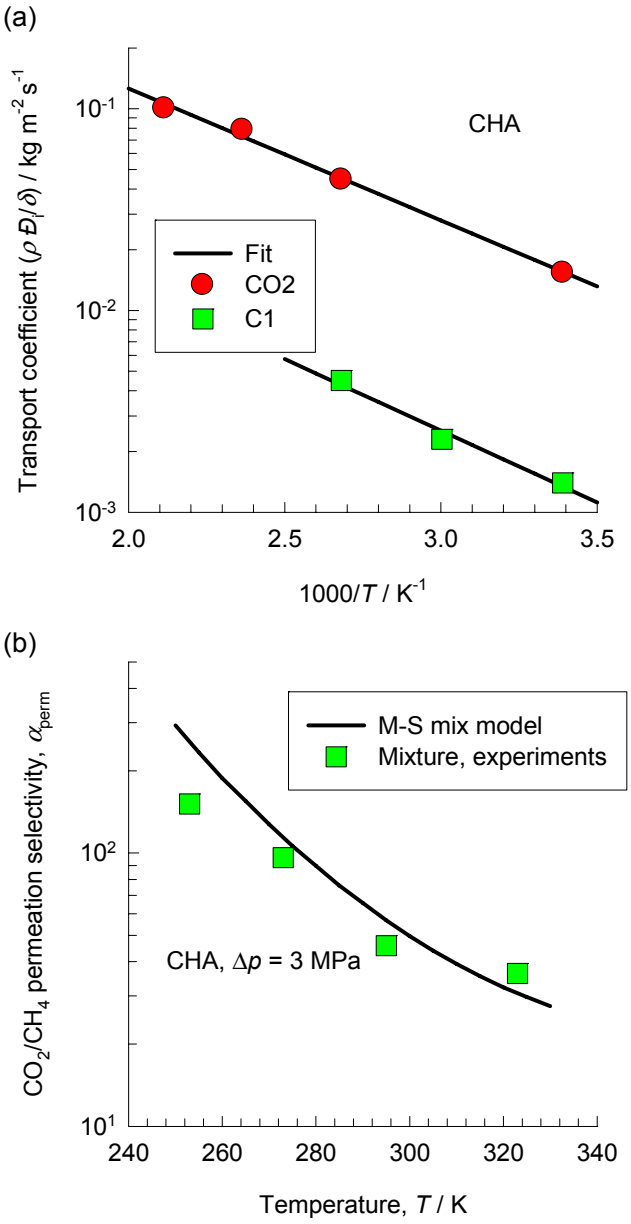
(a)
Transport coefficient ($\rho Đ_i/\delta$) / kg m^{-2} s^{-1}
10^{-1}
10^{-2}
10^{-3}
CHA
Fit
CO2
C1
2.0
2.5
3.0
3.5
1000/T / K^{-1}
(b)
CO_2/CH_4 permeation selectivity, α_{perm}
10^2
10^1
M-S mix model
Mixture, experiments
CHA, Δp = 3 MPa
240
260
280
300
320
340
Temperature, T / K

Figure 4

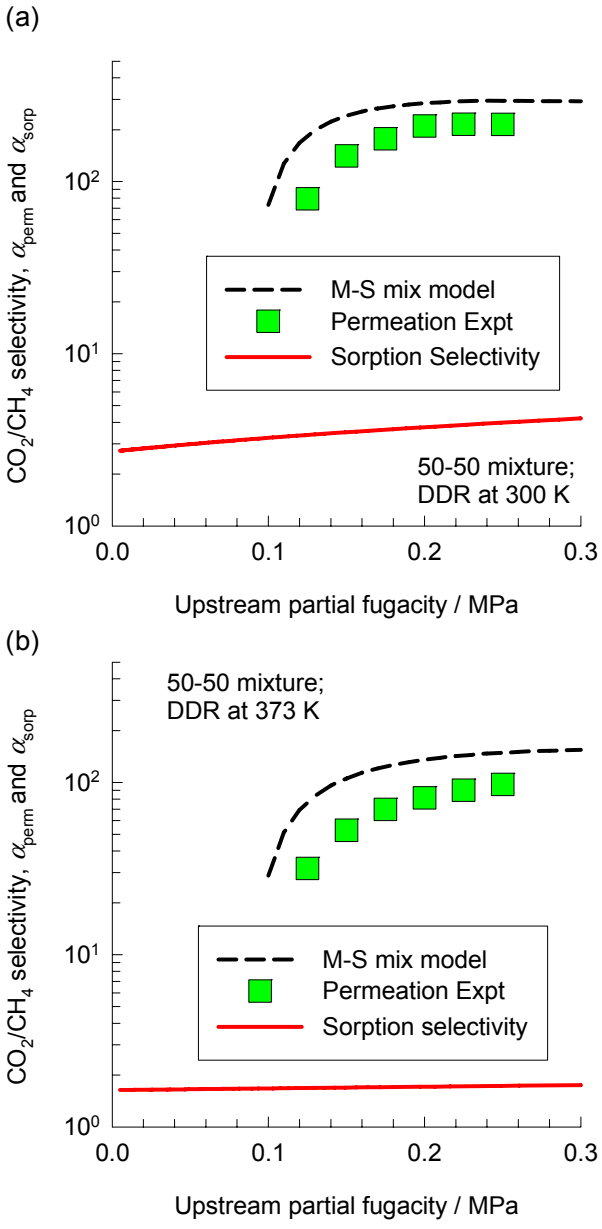
(a)
CO_2/CH_4 selectivity, α_{perm} and α_{sorp}
10^2
10^1
10^0
0.0
0.1
0.2
0.3
M-S mix model
Permeation Expt
Sorption Selectivity
50-50 mixture;
DDR at 300 K
Upstream partial fugacity / MPa
(b)
50-50 mixture;
DDR at 373 K
CO_2/CH_4 selectivity, α_{perm} and α_{sorp}
10^2
10^1
10^0
0.0
0.1
0.2
0.3
M-S mix model
Permeation Expt
Sorption selectivity
Upstream partial fugacity / MPa